Global shape aftereffects in composite radial frequency patterns

Samuel J. D. Lawrence York Neuroimaging Centre, Department of Psychology, University of York, York, UK

Bruce D. Keefe York Neuroimaging Centre, Department of Psychology, University of York, York, UK

Richard J. W. Vernon York Neuroimaging Centre, Department of Psychology, University of York, York, UK

Alex R. Wade York Neuroimaging Centre, Department of Psychology, University of York, York, UK

Declan J. McKeefry University of Bradford School of Optometry and Vision Science, University of Bradford, Bradford, UK

Antony B. Morland York Neuroimaging Centre, Department of Psychology, University of York, York, UK; Centre for Neuroscience, Hull–York Medical School, York, UK

Individual radial frequency (RF) patterns are generated by modulating a circle's radius as a sinusoidal function of polar angle and have been shown to tap into global shape processing mechanisms. Composite RF patterns can reproduce the complex outlines of natural shapes and examining these stimuli may allow us to interrogate global shape mechanisms that are recruited in biologically relevant tasks. We present evidence for a global shape aftereffect in a composite RF pattern stimulus comprising two RF components. Manipulations of the shape, location, size and spatial frequency of the stimuli revealed that this aftereffect could only be explained by the attenuation of intermediate-level global shape mechanisms. The tuning of the aftereffect to test stimulus size also revealed two mechanisms underlying the aftereffect; one that was tuned to size and one that was invariant. Finally, we show that these shape mechanisms may encode some RF information. However, the RF encoding we found was not capable of explaining the full extent of the aftereffect, indicating that encoding of other shape features such as curvature are also important in global shape processing.

Introduction

Recent attention has been drawn to the importance of studying intermediate levels of visual processing (Peirce, 2015). At this stage of processing, the visual image is segregated into distinct objects according to the global shape of each object, which in turn facilitates object recognition (Loffler, 2008). Research has identified curvature as a key visual feature for achieving this segregation (Attneave, 1954; Loffler, 2008; Poirier & Wilson, 2006).

Radial frequency (RF) patterns, stimuli defined by a sinusoidal modulation of a circle's radius as a function of the polar angle (Wilkinson, Wilson, & Habak, 1998), have proven to be powerful stimuli for investigating global shape processing. Importantly, RF patterns have been shown many times to engage global-scale shape processing mechanisms through a range of psychophysical tasks including shape detection (Dickinson, Cribb, Riddell, & Badcock, 2015; Dickinson, McGinty, Webster, & Badcock, 2012; Hess, Wang, & Dakin, 1999; Jeffrey, Wang, & Birch, 2002; Loffler, Wilson, & Wilkinson, 2003; Schmidtmann, Kennedy, Orbach, &

Citation: Lawrence, S. J. D., Keefe, B. D., Vernon, R. J. W., Wade, A. R., McKeefry, D. J., & Morland, A. B. (2016). Global shape aftereffects in composite radial frequency patterns. *Journal of Vision, 16*(7):17, 1–13, doi:10.1167/16.7.17.

doi: 10.1167/16.7.17 Received December 16, 2015; published May 18, 2016 ISSN 1534-7362

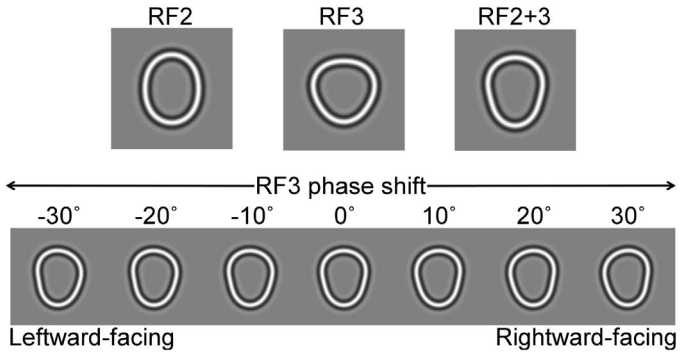

Figure 1. Two RF components with frequencies of two (RF2) and three (RF3) were summed to create an RF2+3 pattern. The shape of this stimulus was manipulated by the phase of the RF3 component, where a phase of 0° created a neutral, front-facing stimulus and increases and decreases in phase resulted in rightward- and leftward-facing rotations, respectively. The RF3 component phases used to create each example stimulus are listed above the stimuli. See text for specific stimulus parameters.

Loffler, 2012; Wilkinson et al., 1998) and shape adaptation (Anderson, Habak, Wilkinson, & Wilson, 2007; Bell, Forsyth, Badcock, & Kingdom, 2014; Bell, Hancock, Kingdom, & Peirce, 2010; Bell & Kingdom, 2009).

One advantage of using RF patterns to study global shape processing is that multiple RF components can be summed to form a single, complex pattern. These composite RF patterns can represent arbitrarily complex boundaries of natural objects such as faces in a convenient, parameterized manner (Wilson, Loffler, & Wilkinson, 2002; Wilson & Wilkinson, 2002; Wilson, Wilkinson, Lin, & Castillo, 2000). They can therefore be used to investigate the contribution of global shape mechanisms to the processing of biologically relevant stimuli.

An example of this is provided by Daar and Wilson (2012) who replicated the face viewpoint aftereffect using synthetic face stimuli generated through a combination of multiple RF components. The face viewpoint aftereffect is a perceptual aftereffect where adaptation to a face rotated away from the observer causes a neutral face to appear rotated in the opposite direction to the adaptor (Fang & He, 2005). Daar and Wilson (2012) showed that adaptation to face outlines alone was sufficient to induce a viewpoint aftereffect in a full-face test stimulus. In doing so, they demonstrated that the shape of a face outline acts as a cue to viewpoint, which is an example of the recruitment of shape processing mechanisms for a biologically relevant task.

In this paper, we introduce a global shape aftereffect in RF2+3 patterns, composite RF pattern stimuli comprising two components with frequencies of 2 (RF2) and 3 (RF3), in which manipulation of the phase of the RF3 component affects shape perceptions. This aftereffect was similar to Daar and Wilson's (2012) synthetic viewpoint aftereffect; however, the use of a simpler combination of RF components allowed us to specifically interrogate the response properties of intermediate-level shape processing mechanisms, which may be recruited for biologically relevant tasks such as viewpoint perception. In addition, the use of a composite RF pattern stimulus allowed us to measure how adaptation to RF3 component phase transfers to different shapes that also include an RF3 component, shedding light on how RF patterns might be processed in the brain. The following series of experiments characterized shape aftereffects in RF2+3 patterns and the neural mechanisms which may underpin them.

We present the results from our experiments in three sections. RF patterns contain shape information which can accurately describe head outlines (Wilson et al., 2000) and these synthetic head outlines are a cue to face viewpoint (Daar & Wilson, 2012). While our stimuli were clearly less complex than a full head outline, they could still give the impression of an abstract head outline changing its viewpoint (see Figure 1), and simple RF pattern stimuli have been shown to elicit responses from face-selective cortex (Wilkinson et al., 2000). We therefore felt it important to first determine whether shape aftereffects in RF2+3 patterns could be explained by genuine viewpoint adaptation encoded by high-level, face-specific mechanisms as opposed to being a lower-level shape aftereffect. Results suggested no engagement of face-specific mechanisms and were consistent with a lower-level shape aftereffect.

Next, we determined whether the aftereffect could be explained by tilt aftereffects by characterizing its sensitivity to stimulus size and spatial frequency. We measured the strength of the aftereffect across a range of test stimulus sizes and spatial frequencies while the adaptor remained constant. The aftereffect exhibited a broad, Gaussian tuning profile to size, plateauing to remain significant across the entire tested range, and complete invariance to spatial frequency. This provided strong evidence that our aftereffect is not a manifestation of tilt aftereffects, which are tuned to spatial frequency (Ware & Mitchell, 1974), and is instead an example of a global shape aftereffect mediated by intermediate-level shape mechanisms. In addition, our results were consistent with other reports of two mechanisms underlying shape aftereffects, one feature-tuned and one feature-invariant (Bell & Kingdom, 2009). We add to these results that feature-tuned mechanisms are tuned to stimulus size but not spatial frequency.

Finally, we asked whether our aftereffect was more consistent with shape encoding by neural channels tuned to RF (Bell & Badcock, 2009) or curvature-based models of global shape perception (Dickinson et al.,

2015; Poirier & Wilson, 2006). We showed evidence to support both alternatives, where adaptation to RF3 phase transferred to test stimuli of different shapes and sizes that contained an RF3 component. However, the magnitude of this effect was not sufficient to account for the entire illusion. We therefore conclude that global shape aftereffects in composite RF patterns constitute adaptation to both RF content and other shape features such as curvature.

General methods

Observers

All observers had normal or corrected-to-normal vision and gave written informed consent. The number of observers for each individual experiment is detailed in the Results section. The experiments were approved by the York Neuroimaging Centre Ethics Committee and adhered to the Declaration of Helsinki.

Stimuli

Two RF patterns (Wilkinson et al., 1998) were summed to generate RF2+3 pattern stimuli (Figure 1). The radius r at polar angle θ for this stimulus was calculated using the following equation:

$$r(\theta) = r_0\Big(1 + A_1\sin(\omega_1\theta + \varnothing_1) + A_2\sin(\omega_2\theta + \varnothing_2)\Big) \quad (1)$$

where r_0 is the mean radius, A_1 and A_2 are the radial modulation amplitudes, ω_1 and ω_2 are the radial frequencies and $\varnothing_1$ and $\varnothing_2$ are the phases of the two RF components. The component stimuli were an RF2 ($\omega_1 = 2$, $A_1 = 0.12$, $\varnothing_1 = -90°$) and RF3 pattern ($\omega_2 = 3$, $A_2 = 0.05$, $\varnothing_2$ variable, where 180° produced a neutral, front-facing stimulus and higher or lower values produced increasingly rightward- or leftward-facing stimuli, respectively). Henceforth, reference to the RF3 component phase will be normalized such that the phase required for a front-facing stimulus will be defined as 0° (as in Figure 1). These stimulus parameters resulted in an RF2+3 pattern whose shape was manipulated using the RF3 component phase (see Figure 1). The cross-sectional luminance profiles of stimulus contours were defined by the following equation:

$$D4(r) = C\left(1 - 4\left(\frac{r - r_0}{\sigma}\right)^2 + \frac{4}{3}\left(\frac{r - r_0}{\sigma}\right)^4\right) \times \exp\left(-\left(\frac{r - r_0}{\sigma}\right)^2\right) \quad (2)$$

where $D4$ is the radial fourth derivative of a Gaussian, C is the contrast, r_0 is the mean radius, and σ is the peak spatial frequency.

Procedure

Stimuli were generated and presented using Psychtoolbox 3.0 (www.psychtoolbox.com) in Matlab v7.14 (MathWorks, Natick, MA) and presented on a gamma-corrected Mitsubishi Diamond Pro 2070^{SB} display (Mitsubishi Electric, Tokyo, Japan) of 1024 × 768 resolution and a refresh rate of 75 Hz on a mid-gray background (49 cd/m^2). Subjects viewed stimuli in a darkened room from a chin rest positioned 57 cm from the display.

The following procedure was used for all experiments except one that used a bias free adaptation paradigm. Any stimulus parameters that deviated from the following are specified in the Results section. The adaptor stimuli were RF2+3 patterns with a mean radius of 2.5° of visual angle and peak spatial frequency of 1.26 c/° whose contrast modulated between −100% and 100% according to a 1 Hz sinusoidal function. At the start of each trial a single adaptor stimulus was presented centrally for 30 s on the first trial and 5 s on subsequent trials. In the baseline adaptation condition adaptor RF3 component phase was 0° (front-facing), while in the adapt-rotated condition the adaptor was rotated to face away from the observer (RF3 component phase = ±12°). The sign of rotation in the rotated adaptor was counterbalanced across participants. After a 1 s interstimulus interval, a test RF2+3 pattern was presented for 200 milliseconds at 50% contrast in the same position as the adaptor. The task was to identify whether the test stimulus was rotated towards the observer's left or right. After the participant responded, the next trial followed a 1.5 s intertrial interval. A pair of 1-up 1-down staircases governed the rotation of the test stimulus in order to estimate point of subjective equality (PSE). The two staircases began at 16° and −16°, with an initial step size of 4°, which halved on reversals 3 to 5. Staircases terminated after 14 reversals. A small (0.5° across) central fixation cross was present through the experiment, except for during the 200 ms test presentation period, and participants were instructed to maintain fixation at all times.

Data analysis

For each adaptation condition, the PSE was calculated by averaging the RF3 component phase of the test stimulus for every trial during the final nine reversals (when step size was minimum) for both staircases. The difference between PSE measurements

from each adaptation condition was a measure of the strength of adaptation. For participants who adapted to a stimulus rotated to the left in the adapt-rotated condition (where a negative PSE shift was predicted), we reversed the sign of both baseline and adapt-rotated PSEs such that any aftereffect in the predicted direction would be represented by a positive shift in PSE.

Results

Shape versus face adaptation

First, we measured whether manipulation of RF3 component phase in the adaptor could affect the perceived shape of RF2+3 patterns. Six observers took part in the experiment (two authors, four naïve). Average PSE measurements were significantly different between adaptation conditions, $t(5) = 9.69$, $p < 0.001$, showing that manipulation of RF3 component phase in the rotated adaptor altered shape perceptions. While our stimuli were simple and contained considerably less shape complexity than real head outlines, we noted that the RF3 phase manipulation shown in Figure 1 gave the impression of an abstract head outline changing its viewpoint. Moreover, RF patterns can elicit responses from face-selective cortex (Wilkinson et al., 2000) and can convey shape cues to face viewpoint (Daar & Wilson, 2012; Wilson et al., 2000). We therefore conducted a series of experiments to determine whether our aftereffect recruited higher-level, face-specific mechanisms encoding the viewpoint of the stimulus, or lower-level shape encoding mechanisms.

Face processing is impaired by stimulus inversion (Freire, Lee, & Symons, 2000; Maurer, Le Grand, & Mondloch, 2002). To establish whether this processing impairment was in any way reflected in our aftereffect, we repeated the experiment using inverted RF2+3 patterns (RF3 component phase increased by 180°; see Figure 2B) in six observers (four naïve). Again, we found a significant aftereffect using inverted RF2+3 patterns, $t(5) = 8.50$, $p < 0.001$. Importantly, there was no significant difference in the magnitude of the aftereffect in upright and inverted stimuli (Figure 2F). The aftereffect was therefore equivalent in both upright and inverted RF2+3 patterns and does not appear to reflect any processing impairment as a result of stimulus inversion.

High-level face aftereffects transfer across large portions of the visual field, remaining significant when stimuli are presented as far as 6° of visual angle from fixation in opposite hemifields (Afraz & Cavanagh, 2008; Zimmer & Kovács, 2011), whereas shape aftereffects do not show this degree of position invariance (Melcher, 2005). This yields a simple prediction: if our aftereffect in RF2+3 patterns recruits high-level face encoding mechanisms, it should transfer across retinal locations. To test this, we measured shape aftereffects in RF2+3 patterns in six observers (four naïve) when adaptor and test stimuli were presented in different quadrants within the same visual hemifield (adapt 5° below and right of fixation, test 5° above and right, see Figure 2C) and when presented in opposite hemifields (adapt 5° right of fixation, test 5° left, see Figure 2D). While we did not measure eye movements, as with all experiments, observers were instructed to maintain fixation throughout the duration of the experiment. In both cases, we found no significant aftereffect, within-hemifield: $t(5) = 1.59$, $p = 0.174$, cross-hemifield: $t(5) = 0.48$, $p = 0.649$. Additionally, aftereffect magnitudes for both experiments were significantly less than those measured using standard and inverted stimuli (Figure 2F). Therefore, unlike high-level face aftereffects, our aftereffect does not transfer across large portions of the visual field, and hence likely involves lower-level shape encoding mechanisms.

Finally, we determined whether we could find similar effects of adaptor RF3 component phase in a completely non–face-like stimulus. To do this, we changed the frequency of the RF2 component to 4 for both adaptor and test stimuli, keeping all other stimulus parameters the same. Resulting RF3+4 patterns did not resemble face outlines, and we measured the effect of RF3 component phase in the adaptor in the same way as for RF2+3 patterns (Figure 2E). In six observers (four naïve), we found a significant aftereffect using RF3+4 patterns, $t(5) = 4.95$, $p = 0.004$, and the magnitude of this effect was not significantly different from standard or inverted aftereffects (Figure 2F). The effect of adaptor RF3 component phase, therefore, is applicable to nonface stimuli such as RF3+4 patterns, and is not specific to shapes that resemble face outlines.

Together, these experiments indicate that our aftereffect in RF2+3 patterns is processed by lower-level shape mechanisms, not higher-level, face-specific mechanisms. However, shape aftereffects may constitute a manifestation of local tilt aftereffects (Dickinson, Almeida, Bell, & Badcock, 2010) rather than true global shape processing. The next series of experiments determined whether our aftereffect could be explained by tilt aftereffects.

Size and spatial frequency tuning

An important aspect of global shape aftereffects is their tolerance to changes in stimulus size between adaptor and test (Anderson et al., 2007; Suzuki, 2001). When stimulus size is changed, the global shape is

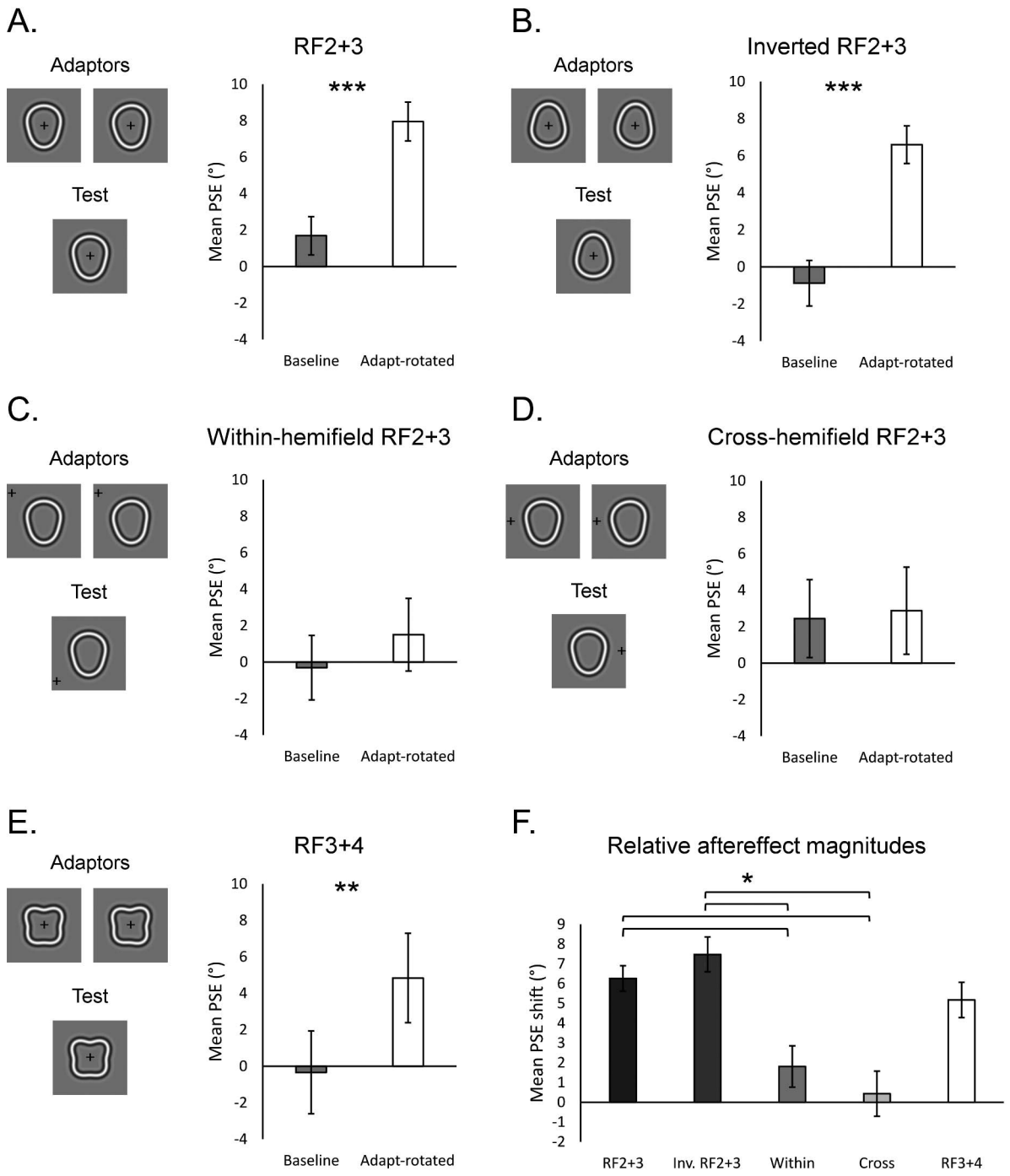

Figure 2. Results from experiments characterizing the processing mechanisms involved in shape aftereffects in RF2+3 patterns. Panels A–E show average PSE measurements for the baseline and adapt-rotated conditions with gray and white bars, respectively, and asterisks denote a significant difference according to a paired-samples *t* test (*** = $p < 0.001$ and ** = $p < 0.01$). Results are shown for (A) upright RF2+3 patterns, (B) inverted RF2+3 patterns, (C) RF2+3 patterns where adaptor and test stimuli were presented in separate quadrants within the same visual hemifield, (D) RF2+3 patterns where adaptor and test stimuli were presented in opposite hemifields, and (E) non–face-like RF3+4 patterns. (F) The average aftereffect magnitude (adapt-rotated PSE minus baseline PSE) is plotted for each of the experiments shown in panels A–E. A repeated-measures ANOVA revealed a significant main effect across experiments, $F(4, 20) = 12.33$, $p < 0.001$, and asterisks denote significant differences according to Bonferroni post hoc tests at the $p < 0.05$ level. In all panels, error bars show standard error of mean.

constant across adaptor and test while each occupies a separate portion of the retinal image. The preservation of a shape aftereffect under these conditions is evidence that it cannot be explained by a simple manifestation of local tilt aftereffects, and that it engages global shape mechanisms that may represent shape by size-invariant stimulus features (Dickinson et al., 2015; Poirier & Wilson, 2006).

We measured our global shape aftereffect in RF2+3 patterns when adaptor and test stimuli had different sizes to ensure it exhibited the same resilience to changes in test stimulus size as other reported shape aftereffects. The mean radius of the test stimulus was 2.1° of visual angle larger than the adaptor (sufficiently large so that there was no contour overlap between adaptor and test stimuli) and the spatial frequency was scaled appropriately using an inverse power law (Figure 3A). In six observers (four naïve), we found a significant difference between PSE measurements from the two adaptation conditions, $t(5) = 10.26$, $p < 0.001$, demonstrating that our aftereffect shows a tolerance to changes in stimulus size similar to other shape aftereffects.

It has been shown that experienced psychophysical observers can voluntarily shift their psychometric functions when instructed to bias themselves (Morgan, Dillenburger, Raphael, & Solomon, 2012). It was therefore argued that some perceptual aftereffects could reflect changes in response bias as opposed to changed perception. This is particularly important when changing stimulus features between adaptor and test as any residual aftereffect could be due to response bias. As a control experiment, we replicated our shape aftereffect in RF2+3 patterns and the effect of stimulus size using a bias free adaptation paradigm (Morgan, 2013).

Three observers (one naïve) completed the bias free experiments. Two adaptors were presented simultaneously, one 4.5° above fixation and the other below, followed by two test stimuli in the same locations. Observers were asked to indicate which of the two test stimuli was more rotated away from the observer. In the baseline condition, both adaptors were front-facing (RF3 phase = 0°), whereas in the adapt-rotated condition the adaptors were rotated in opposite directions to face away from the observer (RF3 phase = ± 20°). There were four possible combinations of test stimulus rotations: both left facing, both right, one left one right, and one right one left. Staircases began at ±20° with an initial step size of 6°, which halved on reversals 1 and 2; data were analyzed using the same methods as described previously. Based on the predicted interactions between adaptors and tests, PSE shifts were predicted for half of the trials and no shifts were predicted for the other half (see Figure 3B and Morgan [2013] for a full description of the paradigm). This process was repeated with test stimuli that were smaller than the adaptors (the size difference was proportionally equal to that used in the test large experiment shown in Figure 3A and spatial frequency was scaled in the same way).

The PSEs measured from shift-predicted trials and no–shift-predicted trails were significantly different for both same size, $t(2) = 6.79$, $p = 0.021$, and small test stimuli, $t(2) = 7.43$, $p = 0.018$. We therefore replicated both the basic aftereffect and the effect of stimulus size using a bias-free adaptation paradigm. It can thus be concluded that global shape aftereffects in RF2+3 patterns and their relative tolerance to changes in stimulus size are due to genuine changes in perception, not changes in response bias. Due to the time-consuming nature of the bias free paradigm (approximately 1.5 hr per participant per condition), the remaining experiments reverted to the standard adaptation paradigm described in the procedure. However, the consistency of our results obtained using bias-free and standard paradigms was taken as evidence that the following experiments measure genuine perceptual effects.

While the aftereffect remained significant with larger and smaller test stimuli, its magnitude was nevertheless reduced compared to the standard aftereffect. This is consistent with other reported effects of stimulus size (Anderson et al., 2007) and suggests that shape aftereffects may exhibit some broad tuning to stimulus size which cannot be appreciated without testing across a broader range. To address this issue and explore the receptive field characteristics of the neural mechanisms underpinning global shape aftereffects, we measured the strength of the aftereffect across a range of size and spatial frequency manipulations.

First, we measured the aftereffect across a broad range of test stimulus sizes while the adaptor size remained constant. The adaptor was presented with a mean radius of 3° of visual angle, and test stimuli were presented over a logarithmic range of mean radii from 33% to 300% of the adaptor with seven levels. All test stimuli were presented with a peak spatial frequency of 2 c/°. For one observer (an author), PSEs were measured for all test stimuli in a single session using interleaved staircases. For the four remaining observers (naïve), data were acquired across four sessions. In three of the four sessions, PSEs were measured for a pair of test stimuli (one smaller than the adaptor, one larger) using interleaved staircases. In the remaining session, PSEs were measured for the test stimulus which was the same size as the adaptor. The ordering of the four sessions and which test stimuli were paired together were counterbalanced across participants.

A 1×7 repeated measures ANOVA revealed a significant main effect of test stimulus size, Huynh-Feldt corrected $F(4.9, 19.6) = 2.97$, $p = 0.038$,

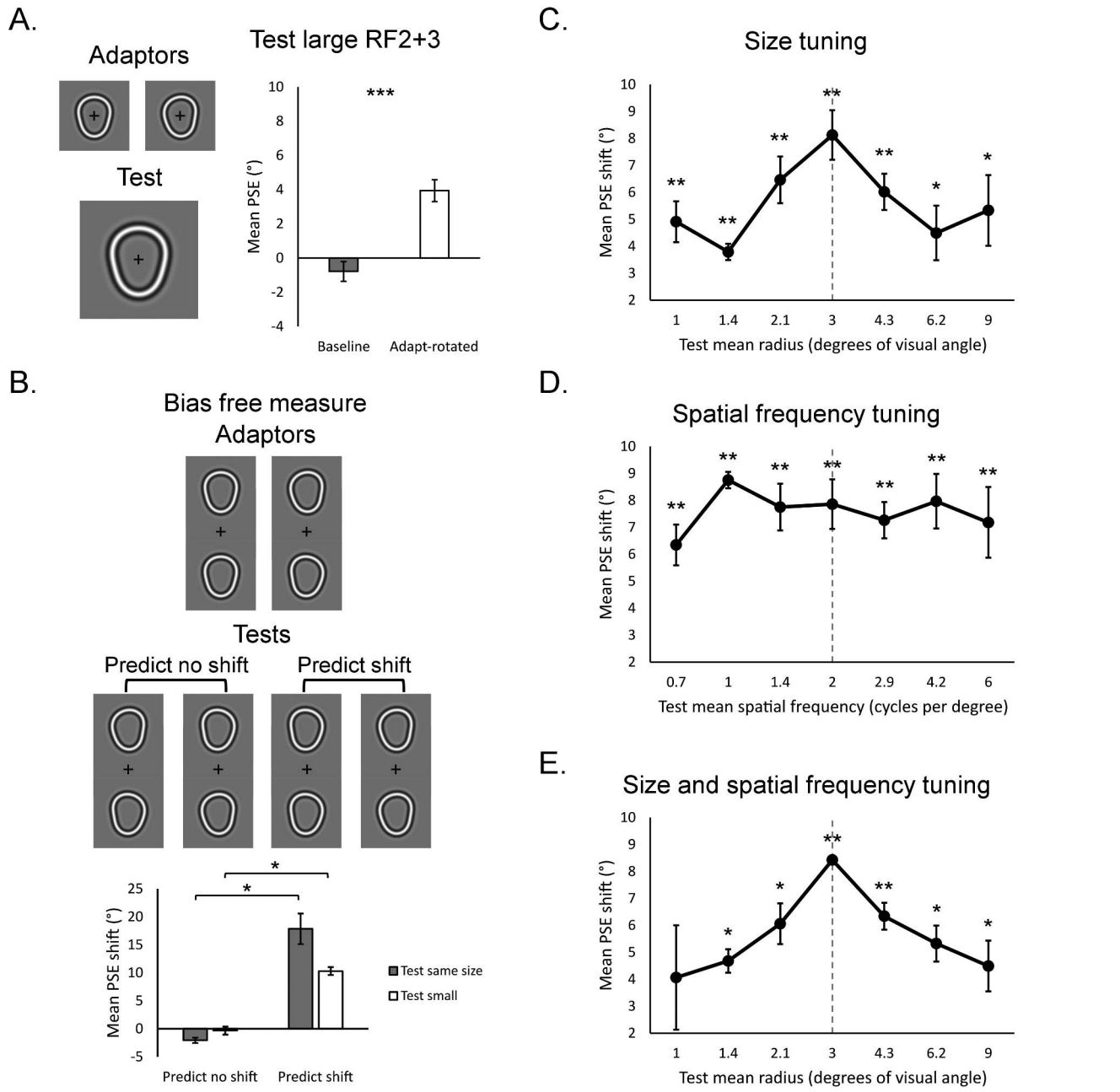

Figure 3. Results from experiments assessing the sensitivity of shape aftereffects in RF2+3 patterns to test stimulus size and spatial frequency. (A) Average PSE measurements are plotted for the baseline (gray bar) and adapt-rotated (white bar) conditions when the test stimulus was larger than the adaptor. A significant difference at the $p < 0.001$ level, according to a paired-samples *t* test, is denoted by ***. (B) Average PSE shifts measured using a bias-free paradigm (Morgan, 2013; see text for further details) are plotted for predict-shift and predict-no shift trials for both same size and smaller test stimuli. A significant difference at the $p < 0.05$ level, according to a paired-samples *t* test, is denoted by *. Panels C–E show average PSE shifts (adapt-rotated PSE minus baseline PSE) for (C) a range of test stimulus sizes, (D) a range of test stimulus spatial frequencies, and (E) a range of test stimulus sizes with scaled spatial frequency. In panels C–E, gray dashed lines indicate the size/spatial frequency of the adaptor and asterisks denote a significant aftereffect according to a one-sample *t* test, where * denotes a significant aftereffect at the $p < 0.05$ level and ** denotes a significant aftereffect using a Bonferroni corrected *p* value of $p < 0.007$. In all panels, error bars show standard error of mean.

demonstrating some level of tuning to test stimulus size. As can be seen in Figure 3C, the tuning profile of the aftereffect across test sizes is broadly Gaussian, peaking when adaptor and test were the same size, and plateaus after a stimulus size difference of approximately 50% or 200%. One-sample *t* tests confirmed that the aftereffect was significantly above zero at the $p < 0.05$ level for all test sizes, where five of seven aftereffects survived a

Bonferroni correction for multiple comparisons (see Figure 3C). The aftereffect, therefore, is systematically reduced by increasing differences in adaptor and test stimulus size until it plateaus, at which point it remains significant in stimuli with size differences of up to a factor of 3.

Tilt aftereffects are tuned to stimulus spatial frequency (Ware & Mitchell, 1974). Therefore, if our aftereffect is driven by tilt aftereffects it should show a similar tuning profile to the cross-sectional spatial frequency of the test stimulus. We measured the tuning of the aftereffect across test stimulus spatial frequencies in four observers (three naïve) using the same methods as for size. Adaptor peak spatial frequency was 2 c/° and test stimuli were presented across a logarithmic range with seven levels as previously explained. All stimuli were presented with the same mean radius (3° of visual angle). The main effect of the test spatial frequency was not significant, Huynh-Feldt corrected $F(4.4, 13.1) = 1.96$, $p = 0.157$, and the tuning profile shown in Figure 3D is relatively flat. Again, all aftereffects were confirmed to be significant (all survived a Bonferroni correction for multiple comparisons; see Figure 3D). It therefore seems that the spatial frequency relationship between adaptor and test stimuli has no effect on the magnitude of the aftereffect.

Finally, we measured the tuning of the aftereffect when test stimulus and spatial frequency varied together in three observers (two naïve). The test stimulus sizes and peak spatial frequencies from the previous two experiments were combined, such that test size and spatial frequency were paired by an inverse power law. While the main effect of test stimulus size and spatial frequency did not reach significance, Huynh-Feldt corrected $F(2.3, 4.7) = 3.60$, $p = 0.111$, this was likely due to weak statistical power from testing only three observers. The tuning profile shown in Figure 3E is similar to that for size tuning in Figure 3C, confirmed by a 2-way repeated measures ANOVA, which found no main effect when comparing the two tuning profiles, $F(1, 2) = 0.05$, $p = 0.851$. The aftereffect was significant for all test stimuli except for the smallest one, two of the six significant aftereffects survived a Bonferroni correction (see Figure 3E). We therefore replicated the broad size tuning of the aftereffect when both size and spatial frequency changed together. Moreover, the similarity of the tuning profiles across the two experiments serves to confirm that test stimulus spatial frequency has no effect on the aftereffect.

Overall, we show that global shape aftereffects in RF2+3 patterns are relatively tolerant to changes in stimulus size, similar to other reported shape aftereffects, which is due to genuine changes in perception rather than response bias. However, when we tested over a broader range of test stimulus sizes, the aftereffect showed a broad Gaussian tuning profile. The aftereffect was also completely invariant to the cross-sectional spatial frequency of the test stimulus across the tested range, and therefore cannot be explained as a manifestation of tilt aftereffects.

Shape versus RF processing

It has been argued that global shape perception may be performed by a bank of narrow-band RF tuned channels that analyze the RF content of an object (Bell & Badcock, 2009). Alternatively, global shape processing may involve an encoding of the shape profile through some form of curvature analysis (Dickinson et al., 2015; Poirier & Wilson, 2006). The following series of experiments were designed to determine whether global shape aftereffects in RF2+3 patterns are more consistent with RF processing, where RF3 component phase is the adapted feature, or shape processing, where the shape profile of the adaptor is the adapted feature.

First, we replicated the RF2+3 pattern shape aftereffect experiment but we removed the RF2 component from adaptor and test stimuli (Figure 4A). Detection thresholds for a target RF are elevated when the target is paired with a mask RF of neighboring frequency to form a composite RF pattern stimulus (Bell, Wilkinson, Wilson, Loffler, & Badcock, 2009). If RF3 component phase is the adapted feature in our shape aftereffect, this should be masked by the presence of the RF2 component in RF2+3 patterns. As such, the magnitude of the aftereffect should be larger in RF3 patterns than RF2+3 patterns. Alternatively, if shape profile is the adapted feature, the aftereffect might be roughly the same in RF3 patterns, as the RF3 phase manipulation has a similar effect on points of maximum curvature in both RF3 and RF2+3 patterns, which are proposed to be the most important shape features in curvature-based models of global shape perception (Dickinson et al., 2015; Poirier & Wilson, 2006).

The aftereffect in RF3 patterns was significant, $t(5) = 7.68$, $p < 0.001$, in six observers (four naïve). More importantly, the magnitude of the aftereffect was almost the same as in RF2+3 patterns, and the difference between them was not significant, $t(5) = .45$, $p = 0.671$ (Figure 4B). Therefore, it appears that the presence of the RF2 component has no masking effect on adaptation to RF3 phase, supporting shape over RF adaptation.

Next, we investigated whether adaptation to RF3 phase could transfer across different shapes. If the aftereffect is driven by the attenuation of RF-tuned channels, adaptation to RF3 phase should affect the perception of different shapes so long as they also contain an RF3 component. As such we measured the

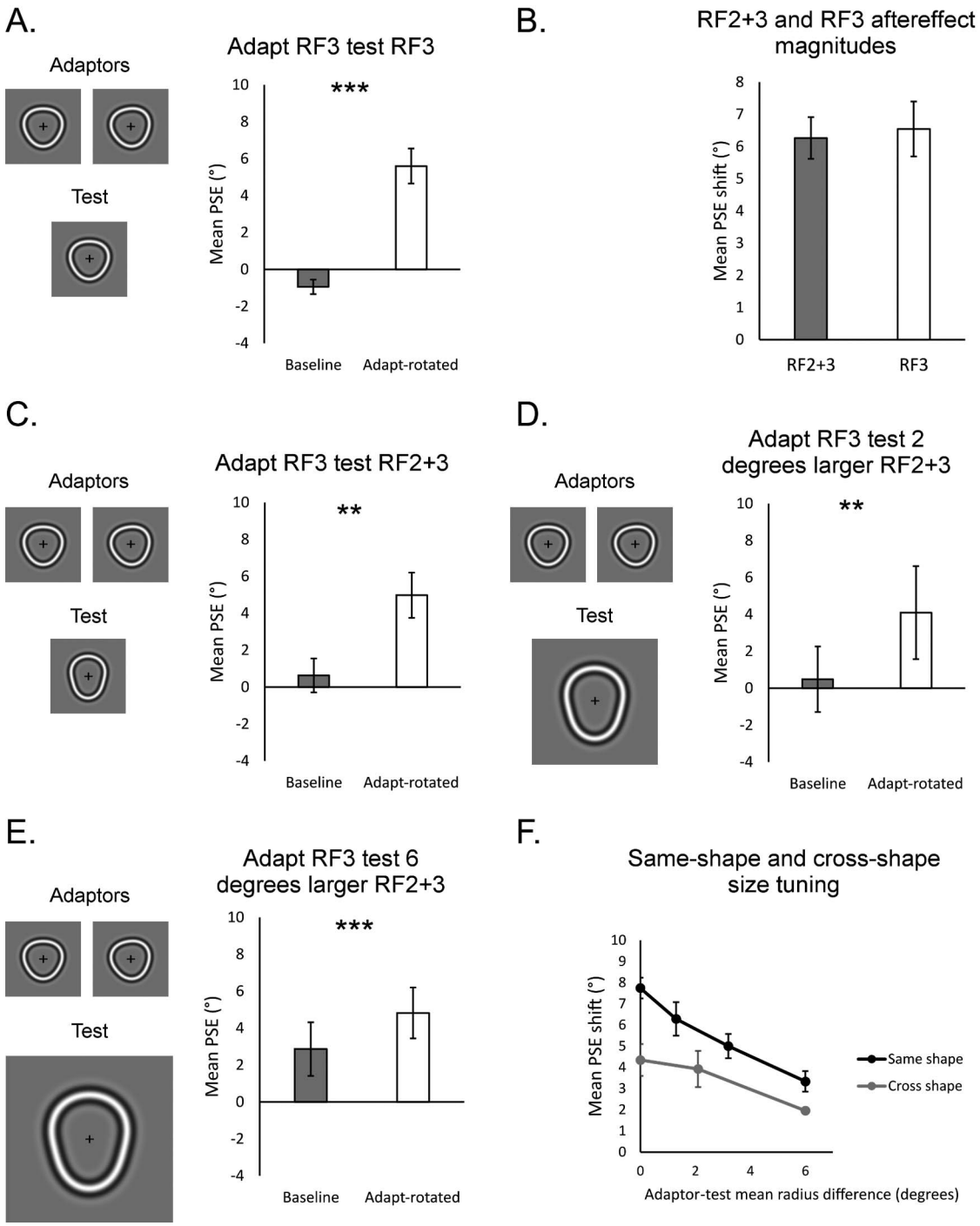

Figure 4. Shape aftereffects assessing the perception of RF3 and RF2+3 patterns following adaptation to RF3 patterns. In panels A and C–E, average PSE measurements for the baseline and adapt-rotated conditions are shown with gray and white bars, respectively, and asterisks denote a significant difference according to a paired-samples *t* test (*** = $p < 0.001$ and ** = $p < 0.01$). (A) Data are shown for RF3 pattern adaptor and test stimuli. (B) The magnitude of the aftereffect shown in panel A (gray bar) is compared with our standard aftereffect in RF2+3 patterns (white bar) derived from the data shown in Figure 2A. In panels C–E, data are plotted for (C) RF2+3 patterns following adaptation to RF3 patterns, (D) RF2+3 patterns that were 2.1° larger than RF3 pattern adaptors, and (E) RF2+3 patterns which were 6° larger than RF3 pattern adaptors. (F) Data from panels C–E are replotted to show cross-shape aftereffect magnitudes as a function of adaptor-test stimulus size differences (gray line) alongside the same function for same-shape aftereffects in RF2+3 patterns (black line; data originally shown in Figure 3E). In all panels, error bars show standard error of mean.

aftereffect in RF2+3 patterns following adaptation to an RF3 pattern (Figure 4C). The aftereffect was significant under these conditions, $t(4) = 5.79$, $p = 0.004$, in five observers (three naïve). The effect of adaptation to RF3 phase, therefore, did transfer to a different shape to affect the perception of an RF2+3 test, supporting RF adaptation.

However, RF3 pattern adaptors and RF2+3 tests were presented in the same location and were the same size. Hence, the observed aftereffect could be due to a manifestation of local tilt aftereffects, which have been argued to be an important and often overlooked component of global shape aftereffects (Dickinson et al., 2010), rather than RF adaptation. To address this, we examined whether this cross-shape aftereffect exhibited the same degree of size invariance as same-shape effects. We conducted two experiments where the adaptor was an RF3 pattern and the test was an RF2+3 pattern that was larger than the adaptor.

For the first experiment the test stimulus was 2.1° of visual angle larger in mean radius than the adaptor and its spatial frequency was scaled (as in the original test large experiment shown in Figure 3A). The aftereffect was again significant, $t(4) = 4.60$, $p = 0.010$ (Figure 4D) in five observers (three naïve). In the second experiment, the test stimulus was 6° larger than the adaptor and its spatial frequency was scaled (equal to the maximum size difference we tested in same-shape aftereffects). The aftereffect was also significant under these conditions, $t(3) = 25.84$, $p < 0.001$ (Figure 4E) in four observers (two naïve). Moreover, the effect of stimulus size is similar in the cross-shape aftereffect to in the same-shape aftereffect, where large size differences reduce the strength of the aftereffect to approximately 50% (Figure 4F). This, therefore, indicates some explicit adaptation to RF3 phase, which transfers across both shape and large differences in stimulus size. However, as shown in Figure 4F the cross-shape aftereffect is clearly reduced in magnitude compared to the same-shape aftereffect. RF3 phase adaptation, therefore, cannot account for the entire illusion, and we thus cannot rule out the contribution of other, more shape-specific mechanisms.

Discussion

We present evidence for a novel class of global shape aftereffect, where manipulation of the phase of a single RF component within a composite RF pattern adaptor affects subsequent shape perceptions. We demonstrated this in RF2+3 patterns where manipulation of the RF3 component phase in the adaptor affected the perceived shape of the test stimulus. Using a range of experiments, we characterized the nature of this aftereffect as well as the shape processing mechanisms that underpin it.

The aftereffect was confirmed to be a lower-level shape aftereffect as opposed to a higher-level face aftereffect. There was no apparent effect of stimulus inversion on the aftereffect and, unlike high-level face aftereffects (Afraz & Cavanagh, 2008; Zimmer & Kovács, 2011), it did not transfer across large portions of the visual field. Moreover, the same RF3 component phase manipulation was used to produce a similar shape aftereffect in RF3+4 patterns, showing the same effect can be induced using non–face-like shapes. Together these results indicate that shape aftereffects in RF2+3 patterns are consistent with the attenuation of shape encoding mechanisms, as opposed to higher-level, face-specific mechanisms.

Shape aftereffects in RF2+3 patterns showed tolerance to changes in stimulus size, remaining significant in stimuli which were larger or smaller than the adaptor. This is consistent with other reported shape aftereffects (Anderson et al., 2007; Suzuki, 2001) and demonstrates global processing as the contours defining adaptor and test stimuli occupied separate portions of the retinal image. It was possible that residual aftereffects measured after stimulus size changes were due to response bias rather than perceptual adaptation (Morgan et al., 2012); however, we ruled this out by replicating the aftereffect and the effect of test stimulus size using a bias free adaptation paradigm (Morgan, 2013). Our shape aftereffect, therefore, taps into the same global shape mechanisms as other shape aftereffects in the literature, and we add that such shape aftereffects reflect genuine changes in perception and cannot be accounted for by simple manifestations of response bias.

Although aftereffects were still present in stimuli of different sizes, they were reduced in magnitude, consistent with other reported effects of stimulus size (Anderson et al., 2007). This suggests some degree of tuning to size, which may not be appreciable when only testing a few stimulus sizes. To address this, we measured the aftereffect across a broad range of test stimulus sizes. The aftereffect exhibited a broad Gaussian tuning profile, peaking when adaptor and test were the same size and declining with increasing size differences until it plateaued, remaining significant in up to size differences of a factor of three. The aftereffect also showed complete invariance to the cross-sectional spatial frequency of the test stimulus across the tested range. Moreover, when test size and spatial frequency were varied together the resulting tuning profile was similar to that for size changes alone, confirming that spatial frequency contributes nothing to the aftereffect. Together, these results demonstrate that our aftereffect cannot be explained by a manifestation of tilt aftereffects, which are tuned to spatial

frequency (Ware & Mitchell, 1974). Therefore, shape aftereffects in composite RF patterns cannot be mediated by high-level face-specific or low-level orientation-specific mechanisms, and instead likely engage intermediate-level shape mechanisms.

The size-tuning profile of our aftereffect constituted both a broad, Gaussian portion and a plateau. This is consistent with the results of Bell et al. (2014), who measured a shape aftereffect in single RF patterns across a range of orientation differences between adaptor and test and found a similar tuning profile with a plateau. Moreover, they provided evidence for two mechanisms, one that was selective for luminance polarity and captured the orientation-tuned portion of the aftereffect, and one that was not selective for luminance polarity and captured the plateau. Our results suggest that the feature-tuned shape mechanism described by Bell et al. (2014) is also tuned to size. In addition, our results indicate that both of these mechanisms are invariant to spatial frequency, implying that the feature-tuned mechanism is invariant to some low-level features. Therefore, both of these mechanisms seem to be involved in some intermediate-level of shape processing, although one is higher-level than the other. Overall, the feature-tuned and feature-invariant components of our aftereffect imply increasingly abstract shape representations, consistent with dimensionality reduction (Wilson & Wilkinson, 2015) and increased complexity of the feature space in which shapes are represented (Güçlü & van Gerven, 2015) through the visual system.

Next, we asked how the intermediate-level shape mechanisms that mediate our aftereffect might encode shape information. Global shape may be represented as a decomposition of the shape profile into its RF components (Bell & Badcock, 2009). Alternatively, shape may be represented by the shape profile determined through some form of curvature analysis (Dickinson et al., 2015; Poirier & Wilson, 2006). We used our global shape aftereffect to disambiguate between these two possibilities. The presence of the RF2 component appears to have no masking effect on adaptation to RF3 component phase in RF2+3 patterns as the aftereffect is of equal magnitude in RF3 patterns and RF2+3 patterns. This provided evidence for shape over RF adaptation as RF components have been shown to have masking effects on the detection of neighboring RFs when presented in a composite stimulus (Bell et al., 2009).

However, we also provide evidence to support adaptation to RF3 component phase as adaptation to an RF3 pattern changed the perception of an RF2+3 pattern test stimulus. Moreover, this cross-shape aftereffect exhibited a similar tuning profile to test stimulus size as same-shape effects, remaining significant in stimuli with size differences of 6°. Therefore, cross-shape aftereffects cannot be accounted for solely by tilt aftereffects and imply the attenuation of RF-tuned channels (Bell & Badcock, 2009). It should also be noted, however, that cross-shape aftereffects were always smaller in magnitude than same-shape aftereffects. As such, RF3 phase adaptation is not sufficient to account for the entire illusion, which is likely mediated by a combination of adaptation to both RF3 phase and other shape features such as curvature.

Finally, our study highlights the possibility that midlevel shape adaptation could contribute to face aftereffects that are often assumed to involve face-specific processes. RF patterns convey shape information, which can describe head outlines (Wilson et al., 2000), act as a cue to face viewpoint (Daar & Wilson, 2012), and elicit responses from face-selective cortex (Wilkinson et al., 2000). Our shape aftereffect in RF2+3 patterns shows some similarities to face aftereffects in the literature. For example, the face distortion aftereffect (Webster & MacLin, 1996) exhibits a similar tuning to stimulus size to our aftereffect, where it is reduced but still significant in stimuli with size differences of up to two octaves (Zhao & Chubb, 2001). These similar results imply that face distortion aftereffects could, at least in part, be explained by shape adaptation. Neural adaptation to faces may also involve shape processing mechanisms. For example, shape adaptation could contribute to neural adaptation to face viewpoint (Fang, Murray, & He, 2007), particularly those effects localized to lateral occipital areas that are known to be shape-selective (Kourtzi & Kanwisher, 2001; Malach et al., 1995). Moreover, neural adaptation to faces in the ventral visual stream has been shown to be invariant to stimulus size, but not to manipulations which affect object shape such as viewpoint (Andrews & Ewbank, 2004). This pattern of results could be consistent with size-invariant global shape mechanisms, implying that shape mechanisms may contribute to neural face adaptation effects. Overall, our results indicate that changing stimulus size is likely not sufficient to isolate face-specific mechanisms, as shape processing mechanisms are tolerant to stimulus size changes. Instead, translation across large portions of the visual field could be used to eliminate the contributions of midlevel shape processing mechanisms.

Conclusions

In conclusion, we show that shape aftereffects in composite RF patterns cannot be explained by high-level, face-specific mechanisms or low-level, orientation-specific mechanisms, and are instead mediated by intermediate-level shape mechanisms. These mechanisms appear to comprise at least two processing

stages. The first is tuned to lower-level stimulus features such as luminance and orientation (Bell et al., 2014), and we add that it is also tuned to stimulus size, but not spatial frequency. The second is invariant to these features and may be the stage at which shapes are represented by size invariant features such as curvature relative to the center (Dickinson et al., 2015; Poirier & Wilson, 2006) or RF content (Bell & Badcock, 2009). We show evidence to support both of these alternatives, and suggest that global shape aftereffects in composite RF patterns are mediated by the attenuation of RF-tuned channels as well as other global shape mechanisms.

Keywords: shape adaptation, radial frequency pattern, global shape processing

Acknowledgments

This research was supported by a Biotechnology and Biological Sciences Research Council (BBSRC) grant #BB/L007770/1 awarded to ABM, ARW, and DJM.

Commercial relationships: none.
Corresponding author: Samuel J. D. Lawrence; Antony Morland.
Email: sjl510@york.ac.uk; antony.morland@york.ac.uk.
Address: York Neuroimaging Centre, Department of Psychology, University of York, York, UK.

References

Afraz, S.-R., & Cavanagh, P. (2008). Retinotopy of the face aftereffect. *Vision Research*, *48*(1), 42–54.

Anderson, N. D., Habak, C., Wilkinson, F., & Wilson, H. R. (2007). Evaluating shape after-effects with radial frequency patterns. *Vision Research*, *47*(3), 298–308.

Andrews, T. J., & Ewbank, M. P. (2004). Distinct representations for facial identity and changeable aspects of faces in the human temporal lobe. *NeuroImage*, *23*(3), 905–913.

Attneave, F. (1954). Some informational aspects of visual perception. *Psychological Review*, *61*(3), 183–193.

Bell, J., & Badcock, D. R. (2009). Narrow-band radial frequency shape channels revealed by sub-threshold summation. *Vision Research*, *49*(8), 843–850.

Bell, J., Forsyth, M., Badcock, D. R., & Kingdom, F. A. A. (2014). Global shape processing involves feature-selective and feature-agnostic coding mechanisms. *Journal of Vision*, *14*(11):12, 1–14, doi: 10.1167/14.11.12. [PubMed] [Article]

Bell, J., Hancock, S., Kingdom, F. A. A., & Peirce, J. W. (2010). Global shape processing: Which parts form the whole? *Journal of Vision*, *10*(6):16, 1–13, doi:10.1167/10.6.16. [PubMed] [Article]

Bell, J., & Kingdom, F. A. A. (2009). Global contour shapes are coded differently from their local components. *Vision Research*, *49*(13), 1702–1710.

Bell, J., Wilkinson, F., Wilson, H. R., Loffler, G., & Badcock, D. R. (2009). Radial frequency adaptation reveals interacting contour shape channels. *Vision Research*, *49*(18), 2306–2317.

Daar, M., & Wilson, H. R. (2012). The face viewpoint aftereffect: Adapting to full faces, head outlines, and features. *Vision Research*, *53*(1), 54–59.

Dickinson, J. E., Almeida, R. A., Bell, J., & Badcock, D. R. (2010). Global shape aftereffects have a local substrate: A tilt aftereffect field. *Journal of Vision*, *10*(13):5, 1–12, doi:10.1167/10.13.5. [PubMed] [Article]

Dickinson, J. E., Cribb, S. J., Riddell, H., & Badcock, D. R. (2015). Tolerance for local and global differences in the integration of shape information. *Journal of Vision*, *15*(3):21, 1–24, doi:10.1167/15.3.21. [PubMed] [Article]

Dickinson, J. E., McGinty, J., Webster, K. E., & Badcock, D. R. (2012). Further evidence that local cues to shape in RF patterns are integrated globally. *Journal of Vision*, *12*(12):16, 1–17, doi:10.1167/12.12.16. [PubMed] [Article]

Fang, F., & He, S. (2005). Viewer-centered object representation in the human visual system revealed by viewpoint aftereffects. *Neuron*, *45*(5), 793–800.

Fang, F., Murray, S. O., & He, S. (2007). Duration-dependent FMRI adaptation and distributed viewer-centered face representation in human visual cortex. *Cerebral Cortex*, *17*(6), 1402–1411.

Freire, A., Lee, K., & Symons, L. A. (2000). The face-inversion effect as a deficit in the encoding of configural information: Direct evidence. *Perception*, *29*(2), 159–170.

Güçlü, U., & van Gerven, M. A. J. (2015). Deep neural networks reveal a gradient in the complexity of neural representations across the ventral stream. *Journal of Neuroscience*, *35*(27), 10005–10014.

Hess, R. F., Wang, Y. Z., & Dakin, S. C. (1999). Are judgements of circularity local or global? *Vision Research*, *39*(26), 4354–4360.

Jeffrey, B. G., Wang, Y. Z., & Birch, E. E. (2002). Circular contour frequency in shape discrimination. *Vision Research*, *42*(25), 2773–2779.

Kourtzi, Z., & Kanwisher, N. (2001). Representation of perceived object shape by the human lateral occipital complex. *Science*, *293*, 1506–1510.

Loffler, G. (2008). Perception of contours and shapes: Low and intermediate stage mechanisms. *Vision Research*, *48*(20), 2106–2127.

Loffler, G., Wilson, H. R., & Wilkinson, F. (2003). Local and global contributions to shape discrimination. *Vision Research*, *43*(5), 519–530.

Malach, R., Reppas, J. B., Beson, R. R., Kwong, K. K., Jiang, H., Kennedy, W. A., & Tootell, R. B. H. (1995). Object-related activity revealed by functional magnetic resonance imaging in human occipital cortex. *Proceedings of the National Academy of Sciences, USA*, *92*, 8135–8139.

Maurer, D., Le Grand, R., & Mondloch, C. J. (2002). The many faces of configural processing. *Trends in Cognitive Sciences*, *6*(6), 255–260.

Melcher, D. (2005). Spatiotopic transfer of visual-form adaptation across saccadic eye movements. *Current Biology*, *15*(19), 1745–1748.

Morgan, M. (2013). Sustained attention is not necessary for velocity adaptation. *Journal of Vision*, *13*(8):26, 1–11, doi:10.1167/13.8.26. [PubMed] [Article]

Morgan, M., Dillenburger, B., Raphael, S., & Solomon, J. A. (2012). Observers can voluntarily shift their psychometric functions without losing sensitivity. *Attention, Perception & Psychophysics*, *74*(1), 185–193.

Peirce, J. W. (2015). Understanding mid-level representations in visual processing vision. *Journal of Vision*, *15*(7):5, 1–9, doi:10.1167/15.7.5. [PubMed] [Article]

Poirier, F. J. A. M., & Wilson, H. R. (2006). A biologically plausible model of human radial frequency perception. *Vision Research*, *46*(15), 2443–2455.

Schmidtmann, G., Kennedy, G. J., Orbach, H. S., & Loffler, G. (2012). Non-linear global pooling in the discrimination of circular and non-circular shapes. *Vision Research*, *62*, 44–56.

Suzuki, S. (2001). Attention-dependent brief adaptation to contour orientation: A high-level aftereffect for convexity? *Vision Research*, *41*(28), 3883–3902.

Ware, C., & Mitchell, D. E. (1974). The spatial selectivity of the tilt aftereffect. *Vision Research*, *14*, 735–737.

Webster, M. A., & MacLin, O. H. (1996). Figural aftereffects in the perception of faces. *Psychonomic Bulletin & Review*, *6*(4), 647–653.

Wilkinson, F., James, T. W., Wilson, H. R., Gati, J. S., Menon, R. S., & Goodale, M. A. (2000). An fMRI study of the selective activation of human extrastriate form vision areas by radial and concentric gratings. *Current Biology*, *10*(22), 1455–1458.

Wilkinson, F., Wilson, H. R., & Habak, C. (1998). Detection and recognition of radial frequency patterns. *Vision Research*, *38*(22), 3555–3568.

Wilson, H. R., Loffler, G., & Wilkinson, F. (2002). Synthetic faces, face cubes, and the geometry of face space. *Vision Research*, *42*(27), 2909–2923.

Wilson, H. R., & Wilkinson, F. (2002). Symmetry perception: A novel approach for biological shapes. *Vision Research*, *42*(5), 589–597.

Wilson, H. R., & Wilkinson, F. (2015). From orientations to objects: Configural processing in the ventral stream. *Journal of Vision*, *15*(7):4, 1–10, doi: 10.1167/15.7.4. [PubMed] [Article]

Wilson, H. R., Wilkinson, F., Lin, L. M., & Castillo, M. (2000). Perception of head orientation. *Vision Research*, *40*(5), 459–472.

Zhao, L., & Chubb, C. (2001). The size-tuning of the face-distortion after-effect. *Vision Research*, *41*(23), 2979–2994.

Zimmer, M., & Kovács, G. (2011). Position specificity of adaptation-related face aftereffects. *Philosophical Transactions of the Royal Society of London. Series B, Biological Sciences*, *366*(1564), 586–595.